Chapter 7

Electrodeposition of Ni-P/SiC Composite Films with High Hardness

Alma Martínez-Hernández, Federico Manríquez-Guerrero, Julieta Torres, Raúl Ortega, José de Jesús Pérez-Bueno, Yunny Meas, Gabriel Trejo and Alia Méndez-Albores

Additional information is available at the end of the chapter

http://dx.doi.org/10.5772/61858

Abstract

This chapter describes the effect of SiC particle concentrations on the metallic continuous phase of the coating and the effect of heat treatment on the crystalline structure, hardness, and wear resistance of electrodeposited Ni-P-SiC coatings. The deposits were obtained via electrodeposition onto an AISI 1018 steel electrode and then heat treated at various temperatures ranging from 300 °C to 600 °C for 60 min in air. The tribological characteristics studied included hardness, friction coefficient, and wear resistance. The results indicated that the dispersion of SiC particles in the metallic matrix improves coating tribological properties such as hardness and wear resistance while diminishing the friction coefficient. The Ni-P-SiC alloy was originally amorphous and was transformed into a mixture of amorphous and crystalline phases when was thermally treated in the range from 400 °C to 500 °C. This phase transformation was associated with the precipitation of a mixture of Ni_3P intermetallic compound and pure Ni crystals. In addition, the results showed that the wear resistance of the Ni-P-SiC coating increased with hardness. The maximum hardness (1453.4 HV) was obtained when the Ni-P-SiC coatings were thermally treated at 500 °C.

Keywords: Ni-P-SiC, electrodeposition, heat treatment, microhardness, wear resistance

1. Introduction

Electrodeposition as an industrial activity has been practiced for over 150 years. Currently, the electrodeposition industry is undergoing fundamental changes as a result of environmental concerns, which increasingly necessitate that certain established plating processes be replaced

with more environmentally friendly technologies. The development of "clean" technologies in the electroplating industry is an essential task required and initiated by environmental protection laws worldwide [1]. From an environmental point of view, chromium (Cr) electrodeposition, which occurs in a wide range of industrial applications in the automotive, aerospace, mining, and petrochemical fields [2], is undoubtedly one of the most damaging electrodeposition processes. In environmental regulations, chromic acid (CrO_3), which is mainly used in hard Cr plating, has been recognized as both highly toxic and carcinogenic and was identified by the U.S. Environmental Protection Agency (EPA) as one of 17 high-priority toxic chemicals [3]. Consequently, the use of hexavalent chromates requires special waste disposal methods and expensive breathing apparatus, and exhaust systems must be employed to address emissions during processing. For these reasons, substitute materials and new designs have been under study for many years. Alloy electrodeposition alternative systems including Ni-W, Ni-P, and Co-W have been considered to replace conventional hard Cr deposition [4,5]. Unfortunately, it is challenging to replace Cr because of its comprehensively favorable material properties, including high hardness, low friction coefficient, and excellent wear and corrosion resistance. A possible approach for the preparation of Ni-based alloy coatings as an alternative to hard Cr is to introduce the new concept of functionally graded deposits (FGDs), which originally evolved from the application of functionally graded materials (FGMs) in which a property gradient arises from position-dependent chemical composition, microstructure, or atomic order [6,7]. Wang et al. [8] found that Ni-P deposits that were heat treated at 400 °C exhibited more than two orders of magnitude higher corrosion resistance than hard Cr deposits. It was found in our previous research that the hardness of Ni-P alloys after heat treatment at 500 °C is close to that of conventional hard Cr [9] and that they exhibited better wear resistance than hard Cr.

Alternatives such as composite coatings have been investigated in recent years. A study on Ni-P-Si_3N_4 composite deposition revealed that increasing the Si_3N_4 content in the deposit greatly increases the hardness and that the wear resistance of the Ni-P-Si_3N_4 composite deposit is four times higher than that of the Ni-P deposit [10]. Other reports [11,12] have concluded that the addition of hard microceramic particles (SiC, Si_3N_4, Al_2O_3, WC, B_4C, BN, CNTs) to the metal matrix can improve its hardness and wear resistance.

An important condition to enhance the hardness of the obtained coatings is by using particles with an average size of less than 1 μm evenly distributed on the surface. In these sense, Guo et al. [13] showed that the presence of carbon nanotubes (CNTs) in the composite coatings improves toughness, strength, and corrosion resistance of the coatings. Likewise, the addition of boron nitride (BN) particles (0.5 μm) to Ni coatings was studied by Pompei et al. [14], and the results showed that Ni-BN coatings present more hardener and wear resistance than those with neat Ni. Similarly, Malfatti et al. [15] found that the incorporation of SiC particles in Ni-P coatings results in higher polarization resistance (lower electrochemical activity) compared to coatings containing only the metallic matrix (Ni-P) for heat-treated specimens. This behavior was associated with a lower superficial active area produced by the nonconductive SiC particles.

http://dx.doi.org/10.5772/61858

Additionally, Zhang et al. [16] and Farzaneh et al. [17] found that Ni-P-SiC composite coatings with high SiC content exhibit better oxidation resistance than Ni-P coatings. Furthermore, Hansal et al. [18] demonstrated that the application of pulse current leads to a more compact composite coating that significantly improves the hardness and tribological behavior of the Ni-P-SiC deposits.

The aim of this work was to study the effect of SiC particle concentrations on the metallic continuous phase of the coating and the effect of heat treatment on the crystalline structure, hardness, and wear resistance of electrodeposited Ni-P-SiC coatings.

2. Materials and methods

2.1. Turbiscan lab expert stability analyses

The obtention of the Ni-P-SiC coatings require the stable dispersion of the SiC particles in the electrolytic bath. An efficient and widely employed method to achieve the effective dispersion of the particles is through the modification of the particle surfaces via the adsorption of a water-soluble polymer [19,20]. The high stability of the suspensions using this methodology is mainly related to electrostatic and steric mechanisms.

The adsorption of cationic surfactant molecules around the SiC particles causes a net positive charge on its surface as a result of increased electrostatic repulsion and steric hindrance between SiCPs. This phenomenon facilitates the migration of the particles toward the surface of the cathode, where they are dispersed during the formation of the Ni-P/SiC coating.

The effect of the surfactant concentration on the stability of SiCPs in an electrolytic bath was studied throughout the next procedure: 0.0625 g of SiC particles (99.9%, 100 nm, SkySpring Nanomaterials, Inc.) was added to 25 mL of a base solution containing 0.2 M NaCl + 0.65 M $NiSO_4 \cdot 6H_2O$ + 0.75 M $NiCl_2$ $6H_2O$ + 0.1 M H_3BO_3 + 0.1 M H_3PO_3 + x mM decyltrimethylammonium bromide (DTAB) (98%, Spectrum Labs, USA) (x = 0.02, 0.04, 0.06, 0.08, 1.00).

The stability of the SiCPs suspended in solution was measured using the methodology describes by Trejo et al. [21]. The typical transmission and backscattering profiles of SiCPs in the electrolytic bath without surfactant CTAB are shown in Figure 1.

2.2. Electrodeposition of Ni-P/SiC composites

Ni-P-SiC electrodeposits were obtained from a modified Watts Ni bath (solution S: 0.15 M H_3BO_3, 2 M NaCl, 0.65 M $NiSO_4 \bullet 6H_2O$, 0.75 M $NiCl_2 \bullet 6H_2O$, and 0.10 M H_3PO_3 with a pH of 1.5 adjusted with 1 M HCl) + 0.084 mM DTAB + x g mL^{-1} SiC (x = 0.00125, 0.0025, 0.005, 0.01, 0.015, or 0.02) using a parallel plate cell with an inter-electrode distance of 5 cm. The solutions were prepared immediately prior to each experiment using deionized water (18 MΩ cm) and analytical-grade reagents of the highest purity available (Sigma-Aldrich). The temperature of the electrolytic bath was controlled at 25 °C. Ni plates (99%, Atotech) were used as the anodes, and a plate of AISI 1018 steel of exposed area 10 × 15 cm^2 was used as the cathode. All reagents were analytical grade.

The electrodeposition current density was selected on the basis of additional tests using a Hull cell. The coatings obtained were of commercial quality, which is suitable for industrial application.

2.3. Morphological and tribological characterization

Crystalline phases were identified by powder X-ray diffraction (XRD) using a Bruker diffractometer model D8 Advance (Bragg-Brentano arrangement, Cu rotating anode). The samples were evaluated over the 2θ range from 30° to 95° at a rate of 0.2° s^{-1}.

Glow discharge spectrometer (GDS) (Leco, Mod. 850A) was employed to obtain elemental composition of the coatings as a function of depth into the coatings.

The coatings hardness value was the average of ten measurements obtained on a Matsuzawa MXT-α7 on the Vickers scale with a load kept at 10 g for 15 s.

A reciprocating ball-on-disk tribometer (CSM tribometer instruments) was used to wear tests. All tests were nonlubricated and carried out under dry at 25 °C temperature and relative humidity of 39%. A 3-mm AISI 8620 ball bearing was used as the counter body under a 2-N load at a sliding speed of 1 cm s^{-1}. The friction coefficient of the three wear tests was recorded, and the wear volume was measured according to the ASTM G99 standard method.

3. Results and discussion

3.1. SiC Particle (SiCP) suspension stability measurements

The transmission profile (Figure 1a) shows a rapid increase in the transmittance signal from the first scans and remains stable in the 1- to 50-mm range. Additionally, the transmittance signal increased with time, a behavior that is indicative of the formation of a clarifying zone in this region (Figure 1b). Additionally, the backscattering profile (Figure 1c) shows an increase in the backscattering signals as a function of time, which is the characteristic of an increase in particle size. This behavior is related to a phenomenon called differential sedimentation [22]. These results revealed that unstable suspensions of SiCPs were obtained when a surfactant was not used.

Figure 2 shows the typical transmission and backscattering profiles of SiCPs in the electrolytic bath with the surfactant DTAB. The transmission profile (Figure 2a) shows increases with time throughout the length of the vial. This increase is more pronounced in the region from 18 to 50 mm, which indicates the formation of a clarifying zone in this region. Furthermore, in the region from 0 to 48 mm, the transmission signals are less than 10% during the first 13 h of the experiment, indicating that the solution is opaque in this range.

The backscattering profile (Figure 2c) shows a decrease in the signals as a function of time, another indication of differential sedimentation [22,23].

The above results revealed that stable suspensions (less than 10% transmission during the first 13 h) of SiCPs were obtained when DTAB was used as a surfactant.

http://dx.doi.org/10.5772/61858

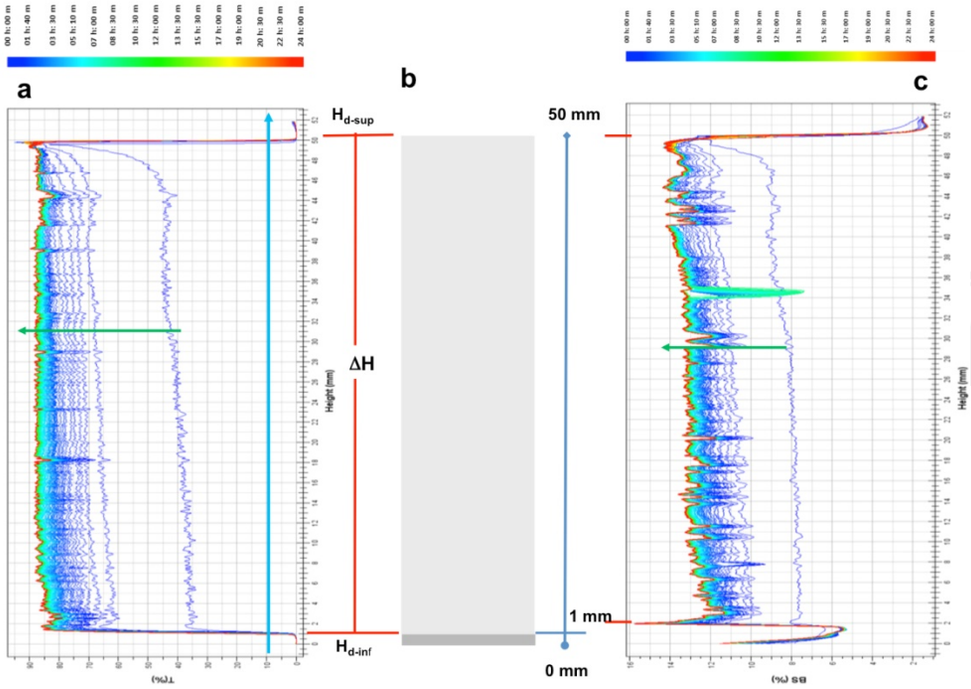

Figure 1. (a) Transmission and (b) backscattering profiles typical of an electrolytic bath of Ni-P-SiC with SiC particles (SiCPs) and without the surfactant DTAB. The data are reported as a function of time (0 to 24 h) and sample height (0 to 50 mm).

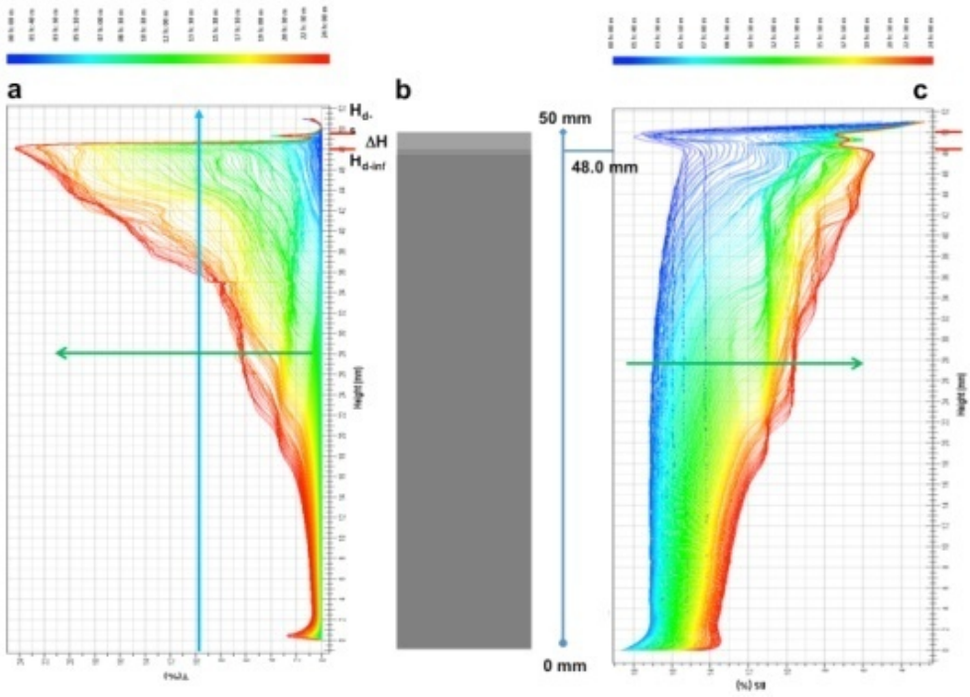

Figure 2. (a) Transmission and (c) backscattering profiles typical of an electrolytic bath of Ni with SiCPs and 0.08 mM CTAB. The data are reported as a function of time (0 to 24 h) and sample height (0 to 50 mm).

Figure 3 shows that the values of the thickness of the clarifying layer (ΔH) in the upper portion of the aqueous SiCP suspension decreased significantly in the presence of the dispersant and increased over time. The best results were obtained for the highest concentrations of CTAB. During the time period from 0 to 13 h, the ΔH value of the aqueous SiCP suspensions with both 0.08 and 0.10 mM CTAB was only 0.85 mm, whereas for the suspension without surfactant, ΔH was 48 mm beginning in the first minutes of the experiment. After 20 h, the ΔH value of the aqueous SiCP suspension with 0.08 mM CTAB was only 6.92 mm.

The greater stability of the SiCPs in the suspension with the dispersant is attributed to the modification of the solid surfaces of the SiC particles via the adsorption of CTAB. Because of its spatial structure and hydrophilic functional groups, CTAB can enhance the electrostatic repulsion and steric hindrance between SiC particles.

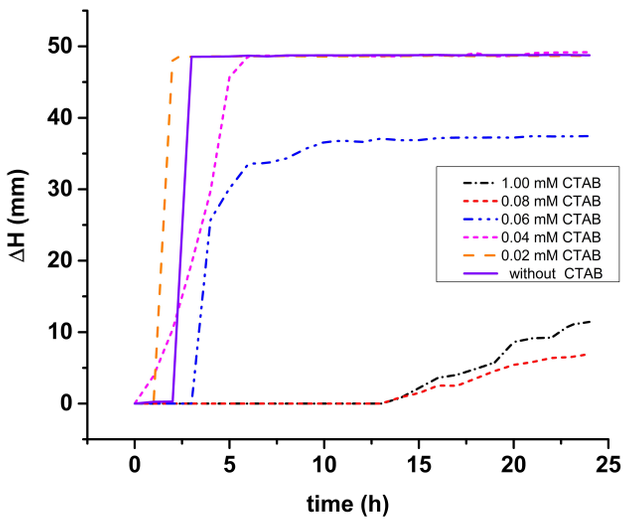

Figure 3. Effect of DTAB dosage on the clarifying-layer thickness (ΔH) as a function of time (0 to 24 h).

3.2. Electrodeposition of composite Ni-P-SiC: Influence of the concentration of SiC particles in solution, on the composition of SiC particles in the matrix Ni-P-SiC composites

3.2.1. Hull cell studies and electrodeposition of Ni-P-SiC composites

A Hull electrochemical cell was used as a first step to find the suitable values of current density that promote uniform coatings of Ni-P-SiC. Prior to the test, an AISI 1018 steel plate was pickled and activated. For pickling, the steel plate was immersed in a 30% HCl solution for 10 s, immediately washed, and then subsequently activated by its immersion in a 10% HCl solution. Immediately after activation, the AISI 1018 steel plate was submerged in a Hull cell containing solution S (= 0.2 M NaCl + 0.65 M $NiSO_4 \cdot 6H_2O$ + 0.75 M $NiCl_2 \cdot 6H_2O$ + 0.1 M H_3BO_3 + 0.1 M H_3PO_3) + 0.084 mM DTAB + x g mL^{-1} SiC (x = 0.00125, 0.0025, 0.005, 0.01, 0.015, or 0.02) (see Figure 4a). Each test was repeated three times for each given SiC concentration. Tests were performed by applying a current of 1 A for 12 min. Ni plates (99%, Atotech) were used as the anodes.

http://dx.doi.org/10.5772/61858

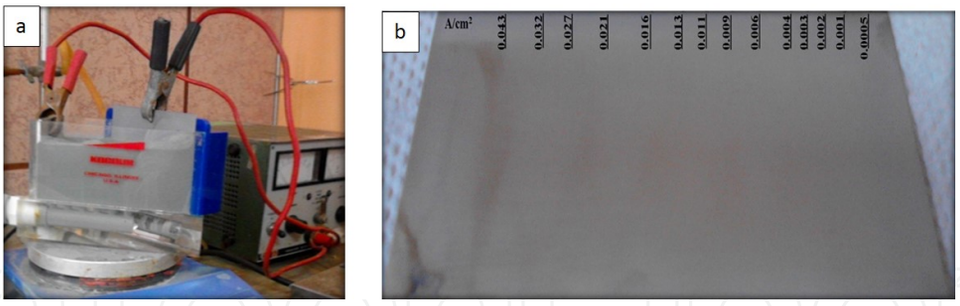

Figure 4. (a) Hull cell containing solution S + 0.084 mM DTAB + 0.02 g mL^{-1} SiC and the AISI 1018 steel plate electrically wired to a power source. (b) Plates with a Ni-P-SiC composite coating obtained after applying 1 A for 12 min.

Figure 4b shows an AISI 1018 steel plate coated with Ni-P-SiC obtained using a solution S + 0.084 mM DTAB + 0.02 g mL^{-1} SiC solution. It was found that current density (j) values between 0.043 and 0.0005 A/cm^2 are adequate to obtain coatings with an appearance and adhesion of acceptable quality.

From this result, Ni-P-SiC coatings were obtained from a solution of composition S + 0.084 mM DTAB + x g mL^{-1} SiC (x = 0.00125, 0.0025, 0.005, 0.01, 0.015, or 0.02) using 1 cm^2 AISI 1018 steel disks as cathodes by applying 0.042 A/cm^2 for 10 min. The obtained coatings are shown in Figure 5. Coatings exhibiting metallic luster were obtained when the solution with the highest concentration of SiC (0.02 g mL^{-1}) was used as an electrolyte.

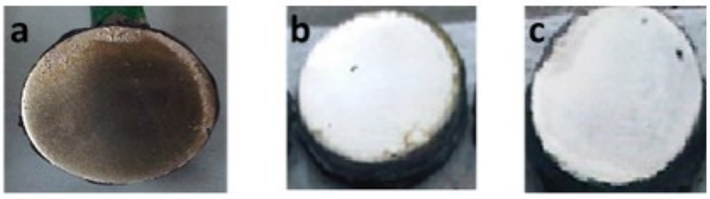

Figure 5. Ni-P-SiC coatings obtained by applying a current density of 0.042 A/cm^2 for 10 min from an electrolytic bath of S (= 0.2 M NaCl + 0.65 M $NiSO_4 \cdot 6H_2$ + 0.75 M $NiCl_2 \cdot 6H_2O$ + 0.1 M H_3BO_3 + 0.1 M H_3PO_3) + 0.084 mM DTAB + x g mL^{-1} SiC, (a) x = 0.02, (b) x = 0.015, (c) x = 0.01.

3.2.2. Characterization of Ni-P-SiC composites

Glow discharge spectroscopy (GDS) was used to obtain the elemental composition profiles of Ni-P-SiC coatings obtained from S solutions having different SiC concentrations. The analysis of the sample was performed at successive depths until the substrate (Fe) was reached.

Figure 6 shows a typical composition profile obtained by GDS. The thickness of the coating was approximately 15 μm. At the surface of the coating, a higher concentration of oxygen was present, presumably indicating surface oxidation. After the oxide layer was removed from the surface, Ni, P, Si, and C were observed; in the range of 2.5 to 25 μm, the composition of Ni and P changed slightly as a function of depth, whereas the Si concentration remained constant but increased inside the AISI 1018 steel matrix. Additionally, the oxygen concentration decreased. A similar behavior was observed for all the SiC concentration values tested.

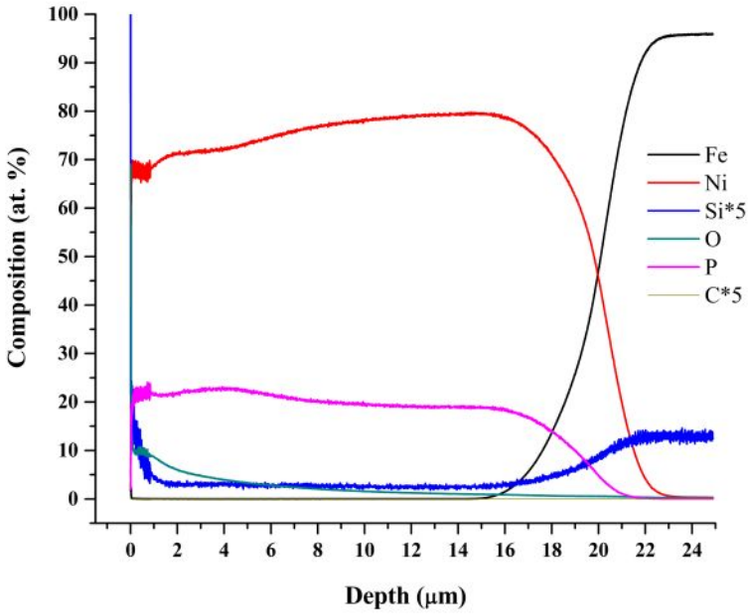

Figure 6. Typical GDS elemental composition profiles of Ni-P-SiC coatings electrodeposited at 0.042 mA/cm^2, t = 10 min from solutions S (0.2 M NaCl + 0.65 M $NiSO_4 \cdot 6H_2O$ + 0.75 M $NiCl_2 \cdot 6H_2O$ + 0.1 M H_3BO_3 + 0.1 M H_3PO_3) + 0.084 mM DTAB + 0.02 g mL^{-1} SiC.

Figure. 7 shows the variation of the SiC content in the coating matrix as a function of SiC concentration in the electrolytic bath. With an increase in SiC concentration in the solution, the concentration of SiC dispersed in the obtained coating increases until a maximum value of 0.6 at.% is reached when a solution with a SiC concentration of 0.015 g/mL is used. With higher concentration values, the percentage of SiC in the coating matrix decreases.

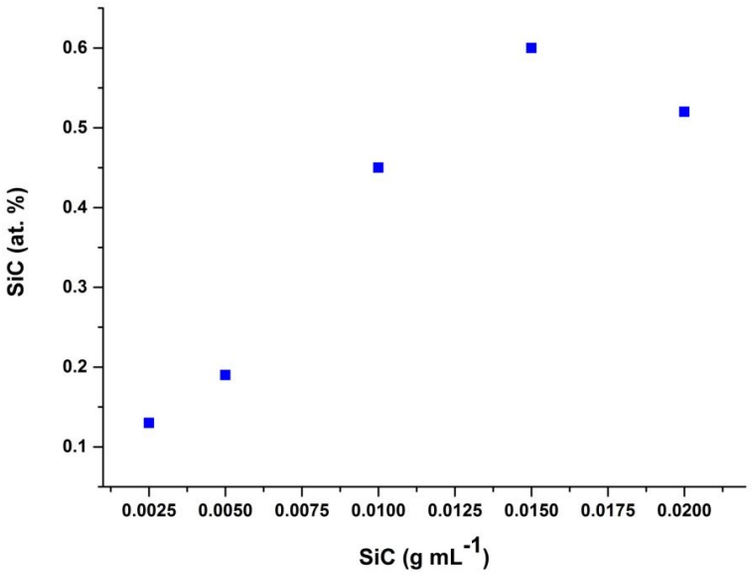

Figure 7. Change in the SiC concentration in the Ni-P-SiC coating matrix as a function of the SiC concentration in the solution. Coatings were obtained at 0.042 mA/cm^2, t = 10 min.

http://dx.doi.org/10.5772/61858

Figure 8 shows the XRD patterns obtained for Ni-P-SiC coatings having different SiC concentrations in the metallic matrix. The peaks that correspond to different crystallographic orientations of Ni are most prominent. No significant changes were found in the Ni XRD patterns recorded for coatings with different SiC concentrations in the metallic matrix.

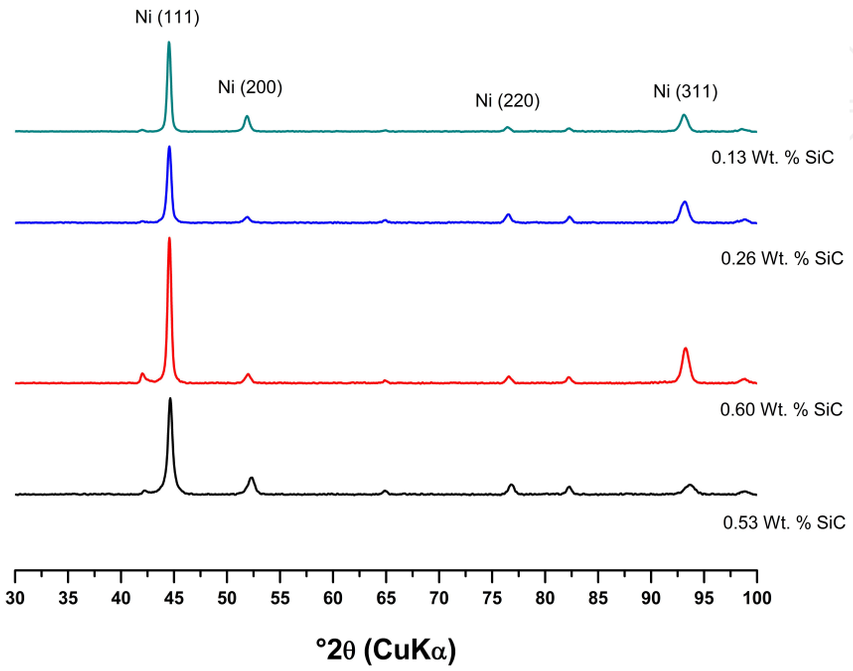

Figure 8. XRD patterns for Ni-P-SiC coatings with different SiC contents in the metallic matrix that were electrodeposited onto AISI 1018 steel.

3.2.3. Microhardness of Ni-P-SiC electrodeposits

The microhardness of the Ni-P-SiC coatings with different SiC concentrations was measured. Figure 9 illustrates the surface microhardness of the electrodeposited Ni-P-SiC coatings as a function of the SiC concentration in the metallic matrix. As observed from the curve, the hardness of the coating increases to values in the range of 580 to 620 HV when SiC particles are dispersed in the metallic matrix. This behavior is associated with increased hard sites. Despite such increases, the obtained hardness was less than that of a hard Cr coating, which has a microhardness of 1020 HV [24].

3.2.4. Wear resistance

To understand the wear mechanism of the electrodeposited Ni-P-SiC composite coatings, the wear track patterns were studied by SEM. As shown in Figure 10, there were many adhesive tearing and plough lines in the sliding direction. Compared to the other Ni-P-SiC coatings, the coating with 0.52 at.% SiC (Figure 10e) exhibited the narrowest and shallowest plough lines. These findings indicated that the coating with 0.52 at.% SiC had the best wear resistance.

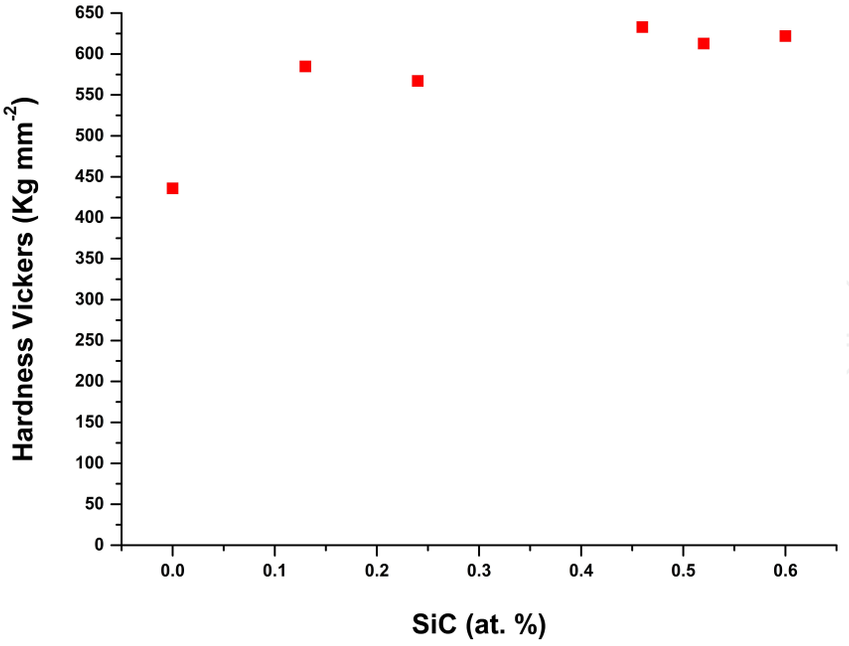

Figure 9. Hardness of the electrodeposited Ni-P-SiC coatings depending on the concentration of SiC in the metallic matrix.

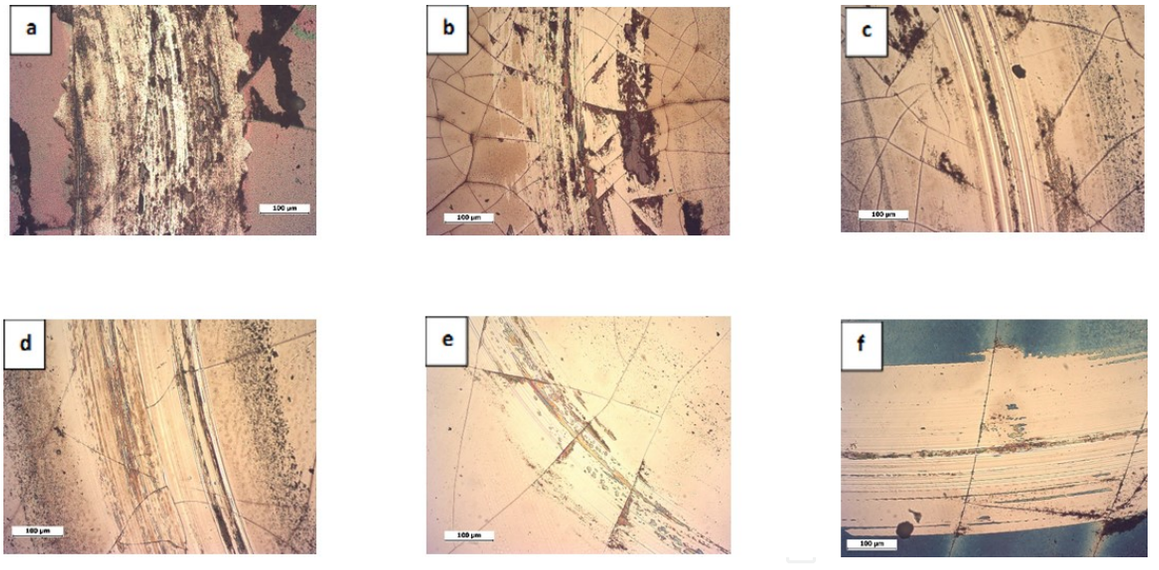

Figure 10. SEM images of wear track of Ni-P-SiC coatings, with different SiC at.% after sliding against AISI 8620 ball in air: (a) 0.0, (b) 0.13, (c) 0.24, (d) 0.46, (e) 0.52, (f) 0.60 at.% SiC.

Figure 11 shows the curves of the wear volume of the electrodeposited Ni-P-SiC coatings as a function of the content of SiC in the metal matrix. The presence of SiC in the metallic matrix of the coating decreases volume wear. The lowest wear volume value was obtained when the SiC concentration in the metallic matrix of the Ni-P-SiC coating was 0.52 at.%. Wear volume values for the other tested concentrations were in the range of 150 to 200 $\mu m^3\ N^{-1}m^{-1}$.

http://dx.doi.org/10.5772/61858

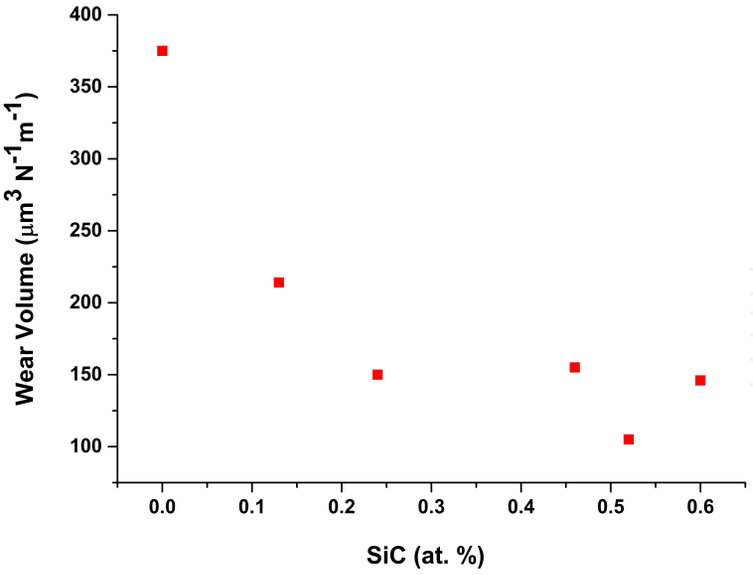

Figure 11. The wear volume of the Ni-P-SiC coatings as a function of the content of SiC in the metal matrix.

3.2.5. Friction coefficients

Figure 12 shows the behavior of the values of the friction coefficients of the Ni-P-SiC coatings obtained. After 5000 cycles, the coating Ni-P-SiC with 0.6 at.% had the lowest value of friction coefficient (0.12 μ), which is similar to the value measured for a hard Cr coating (0.11 μ).

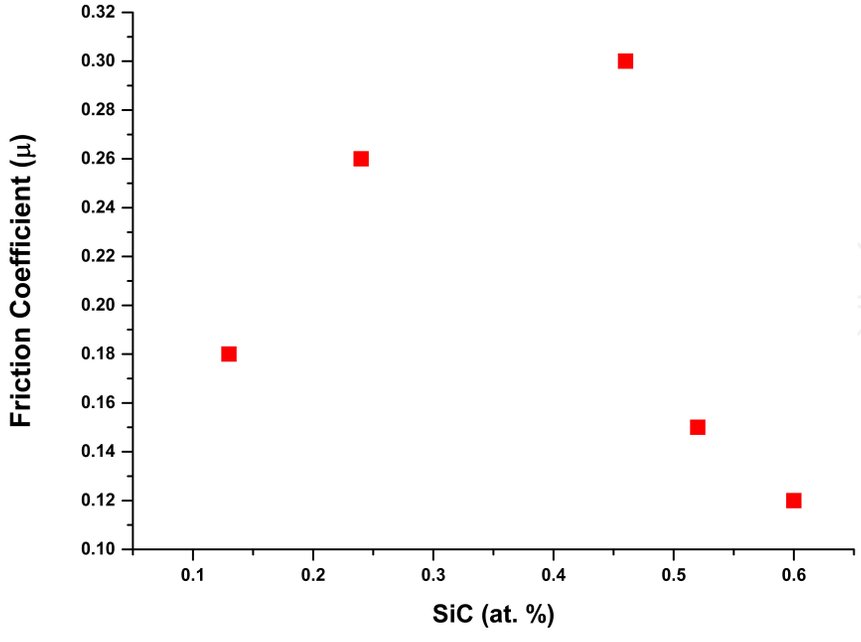

Figure 12. Variation of friction coefficient values as a function of the SiC (at.%) concentration in Ni-P-SiC composite coatings.

3.3. Effects of heat treatment on the tribological properties of electrodeposited Ni-P-SiC composites

Over the last two decades, a variety of surface engineering processes have been developed to enhance the wear resistance, hardness, and corrosion performance of materials. Today, Ni-P alloys are widely used in the aerospace, automotive, and electronic industries because they possess a high degree of hardness, wear resistance, and corrosion resistance, as well as a low friction coefficient [25–28]. In this regard, Malfatti et al. [29] found that the transition from crystalline to amorphous structures occurs progressively over the range of several atomic percent of P and that as-deposited Ni-P coatings are amorphous when the P content exceeds 15 at.%. In contrast, the amorphous alloys can be crystallized via heat treatment, followed by decomposition to nickel phosphide (Ni_3P) and face-centered cubic (fcc) Ni crystals at temperatures above 350 °C [30]. The tribological characteristics of the Ni-P coatings can generally be improved via an appropriate heat treatment [31–33], which can be attributed to precipitation of fine Ni crystallites and hard intermetallic Ni_3P particles during the crystallization of the amorphous phase [34]. In this respect, the wear resistance of the Ni-P alloys increases after heat treatment [35]. Moreover, Wang et al. [8] recently showed that Ni-P electroless coatings heat treated at 400 °C exhibited corrosion resistances of over two orders of magnitude better than hard Cr deposits.

The aim of this section was to study the effects of heat treatment on the physical properties of electrodeposited Ni-P-SiC coatings, including their crystalline structure, hardness, and resistance to wear.

3.3.1. Materials and methods

Ni-P-SiC electrodeposits were obtained from a modified Watts Ni bath (containing 0.2 M NaCl, 0.65 M $NiSO_4 \cdot 6H_2O$, 0.75 M $NiCl_2 \cdot 6H_2O$, 0.1 M H_3BO_3, 0.1 M H_3PO_3 [36]) + 0.084 mM DTAB + 0.02 g mL^{-1} SiC, with a pH of 1.5 adjusted with 1 M HCl) (solution S_1). These solutions were prepared immediately prior to each experiment using deionized water (18 MΩ cm) and analytical-grade reagents of the highest purity available (Sigma-Aldrich).

The Ni-P-SiC coatings were obtained via electrodeposition of solution S_1 under galvanostatic conditions. The coatings were then annealed in air for 60 min at one of four temperatures: 300 °C, 400 °C, 500 °C, or 600 °C.

An atomic force microscope (AFM) (Digital Instruments, Mod. Nanoscope E) was used in contact mode to image the deposited Ni-P-SiC on the steel substrate. These measurements were performed in air (ex situ) using silicon nitride AFM tips (Digital Instruments). All images were obtained at 2 Hz and are represented in the so-called height mode, in which the highest portions appear brighter.

The deposited phases were identified via X-ray diffraction (XRD) using a Bruker diffractometer (Mod. D8 Advance) (Bragg-Brentano arrangement) with CuKα radiation (λ = 1.54 Å). The range of 2θ from 40° to 95° was recorded at a rate of 0.2° s^{-1}.

http://dx.doi.org/10.5772/61858

The elemental composition of the coatings as a function of the thickness was obtained using a glow discharge spectrometer (GDS) (Leco, Mod. 850A).

Hardness was measured with a Matsuzawa MXT-ALFA Vickers microhardness tester with a 10-g load applied for 15 s. The final value quoted for the coating hardness was the average of ten measurements.

Wear tests were performed on a reciprocating ball-on-disk tribometer (CSM tribometer) in air at a temperature of approximately 25 °C and a relative humidity of approximately 39% under dry, nonlubricated conditions. Balls (3 mm diameter) made of AISI 8620 with a hardness of 25 HRC were used as the counter body in the wear tests. All wear tests were performed under a 2-N load at a sliding speed of 1 cm s^{-1}. The friction coefficient and the sliding time were automatically recorded during the test. The wear volume was measured according to the ASTM G99 standard method. Three wear tests were conducted for each sample.

3.3.2. Results

3.3.2.1. Electrodeposition of Ni-P-SiC composites

Hull cell tests were performed using an S solution + 0.084 mM DTAB + 0.02 g/mL SiC, an applied current of 1 A, and a test time of 12 min. Each test was repeated three times. The typical behavior obtained for this system is shown in Figure 13.

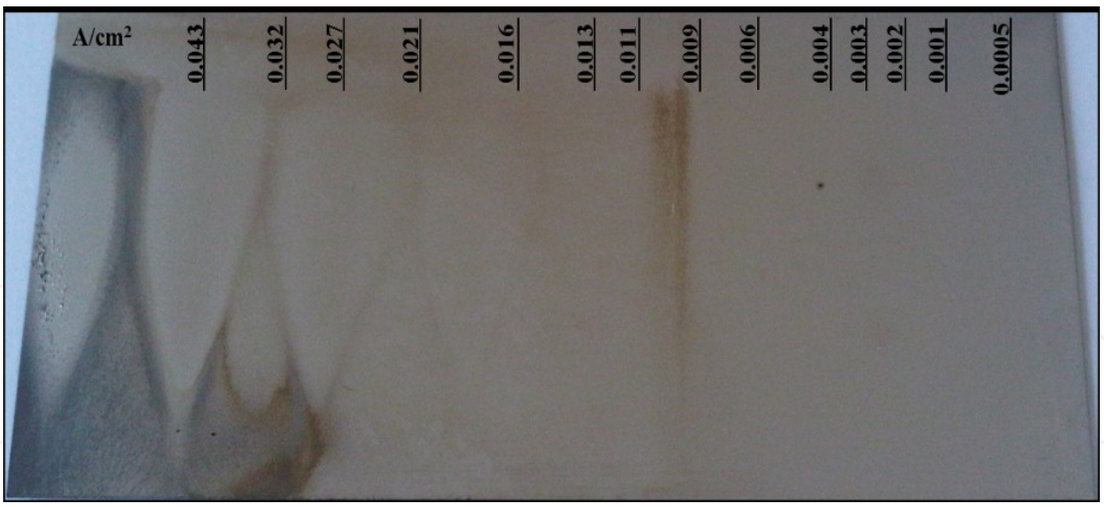

Figure 13. Surface morphology of Ni-P-SiC composite deposited by a Hull cell, i = 1 A, t = 12 min, obtained from solution S + 0.084 mM DTAB + 0.02 g mL^{-1} SiC.

Figure 13 indicates that homogeneous coatings can be obtained when current densities (j) between 0.021 and 0.003 A cm^{-2} are applied. These results demonstrate that 20 μm thick Ni-P-SiC coatings can be obtained by applying 0.021 A cm^{-2} for 20 min. The obtained coating is shown in Figure 14. Ni-P-SiC coatings obtained through the parallel plate technique are of metallic appearance, are well attached, and exhibit metallic luster.

Figure 14. Surface morphology of Ni-P-SiC composite obtained from an S solution (= 0.2 M NaCl, 0.65 M $NiSO_4 \cdot 6H_2O$, 0.75 M $NiSO_4$ $6H_2O$, 0.1 M H_3BO_3, 0.1 M H_3PO_3) + 0.084 mM DTAB + 0.02 g mL^{-1} SiC and j = 0.021 A/cm^2 for 20 min.

3.3.2.2. Thermal treatment

The Ni-P-SiC composite coatings obtained in the previous section were thermally annealed at different temperatures: 300 °C, 400 °C, 500 °C, and 600 °C for 60 min. Each test was repeated three times for each temperature set point.

Figure 15 shows the Ni-P-SiC plates after annealing. Annealed Ni-P-SiC coatings exhibit evident changes in surface morphology with respect to their nonannealed counterparts (see Figure 14).

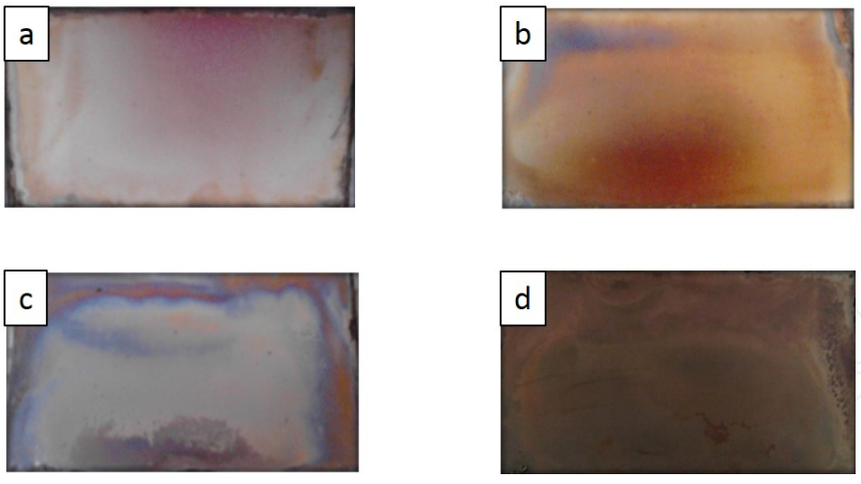

Figure 15. Surface morphology of Ni-P-SiC composite coatings after thermal annealing at (a) 300 °C, (b) 400 °C, (c) 500 °C, and (d) 600 °C.

3.3.2.3. Glow discharge spectroscopy characterization

Figure 16 shows the typical concentration profile of a Ni-P-SiC coating after thermal annealing. The oxygen found on the coating surface is associated with superficial oxidation. After removing the oxide layer, a constant composition of Ni and P is observed through the entire

coating thickness (24 μm). The Si concentration, however, is lower in the upper layers of the coating (5 to 22 μm) and increases in the deeper layers (22.5 to 25 μm). A similar behavior was observed for all the analyzed coatings.

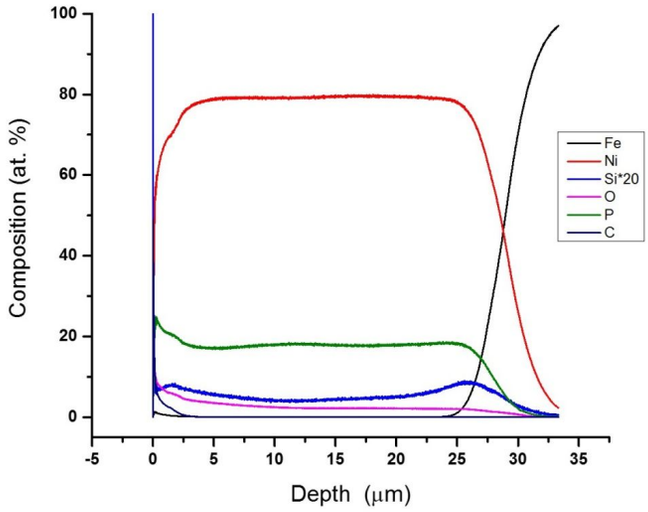

Figure 16. GDS elemental distribution profiles of a Ni-P-SiC coating after thermal annealing and electrodeposited under galvanostatic conditions (j = 0.021 A/cm^2, t = 20 min) in solution S + 0.084 mM DTAB + 0.02 g mL^{-1} SiC.

Table 1 shows the variation of SiC content in the Ni-P-SiC coating matrix after thermal annealing at different temperatures. A decrease in Si content is observed on thermally treated coatings. An approximate 57% loss of Si was observed in the range of 300 °C to 500 °C and increased to 70% when the coating was annealed at 600 °C. This observed behavior could be related to the detachment of SiC particles from the coating matrix during thermal annealing, which is corroborated by composition profile analysis. GDS composition profiles show that the SiC composition remains constant inside a certain range of the coating thickness but increases at the deepest point. This indicates that SiC particle detachment occurs in the upper and middle coating layers.

Annealing Temperature / °C	0.0	300	400	500	600
at. % Si	0.77	0.33	0.32	0.39	0.23

Table 1. Atomic percentages of Si in the Ni-P-SiC composite coatings after 60 min thermal annealing at different temperatures.

3.3.2.4. XRD characterization

Figure 17 shows the XRD patterns for the Ni-P-SiC coatings without heat treatment and with heat treatment (60 min) at different temperatures. Without heat treatment and at annealing temperatures below 400 °C, only a small broad peak appears in the XRD patterns, suggesting

an amorphous structure without phase transition. However, when the heat treatment temperature was close to 500 °C, the structure became crystalline and the XRD pattern shows new sharp peaks corresponding to crystalline fcc Ni (JCP2 04-0850) and Ni_3P (JCP2 89-2743). The transition can be related to the crystallization of neat Ni and the consecutive precipitation of Ni_3P from the supersaturated Ni-P solid solution [30,13,37-38]. Studies of similar systems [39–41] have established that amorphous Ni-P alloys are less dense than crystalline Ni-P alloys, and as consequence, the transition from amorphous to crystalline structure is accompanied by a volume contraction [13]. In agreement with this statement, after the thermal treatment at 500 °C of the Ni-P-SiC composites, a signal corresponding to SiC particles appears.

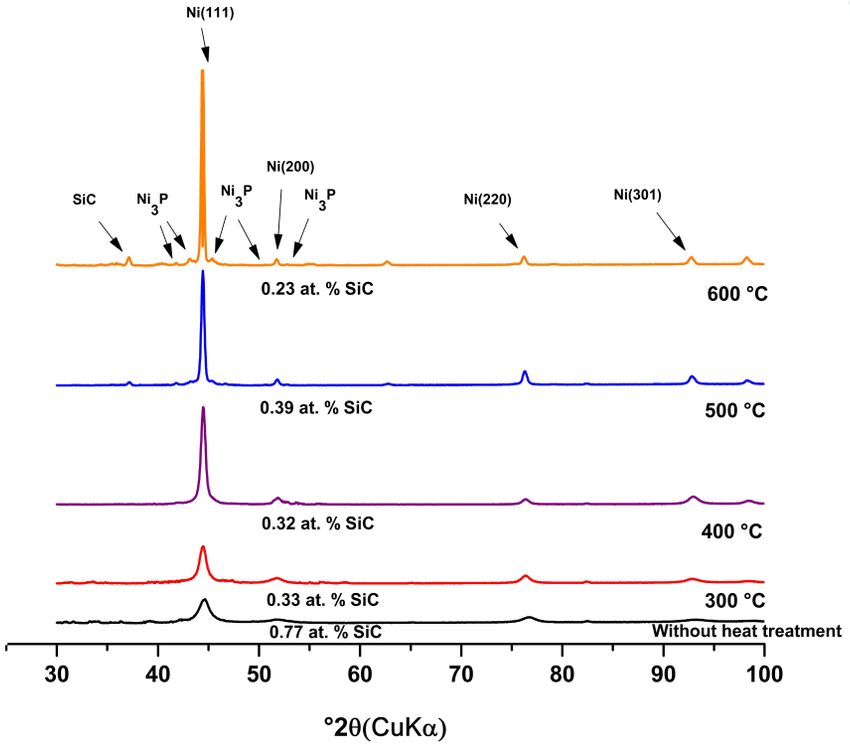

Figure 17. XRD patterns for Ni-P-SiC coatings electrodeposited onto AISI 1018 steel and heat treated at different temperatures. Ni (JCP2 04-0850) and Ni_3P (JCP2 89-2743).

3.3.2.5. AFM characterization

AFM in contact mode was used to obtain images of the Ni-P-SiC coatings both with and without heat treatment for 60 min at different temperatures. Figure 18 shows the AFM images obtained from Ni-P-SiC coatings thermally treated at different temperatures: without thermal annealing, 300 °C, 400 °C, 500 °C, and 600 °C. When the coating was treated at 300 °C (Figure 18b), an amorphous structure containing some crystals was observed; these crystals are associated with the initial formation of the Ni_3P species. At 500 °C (Figure 18d), a larger quantity of crystals associated with the formation of the Ni_3P species was observed in addition to smaller crystals corresponding to fcc Ni. Finally, at 600 °C (Figure 18e), the entire surface was covered with Ni_3P and Ni crystals. These results confirm the phase transition and formation of the Ni_3P and fcc Ni species observed by XRD.

http://dx.doi.org/10.5772/61858

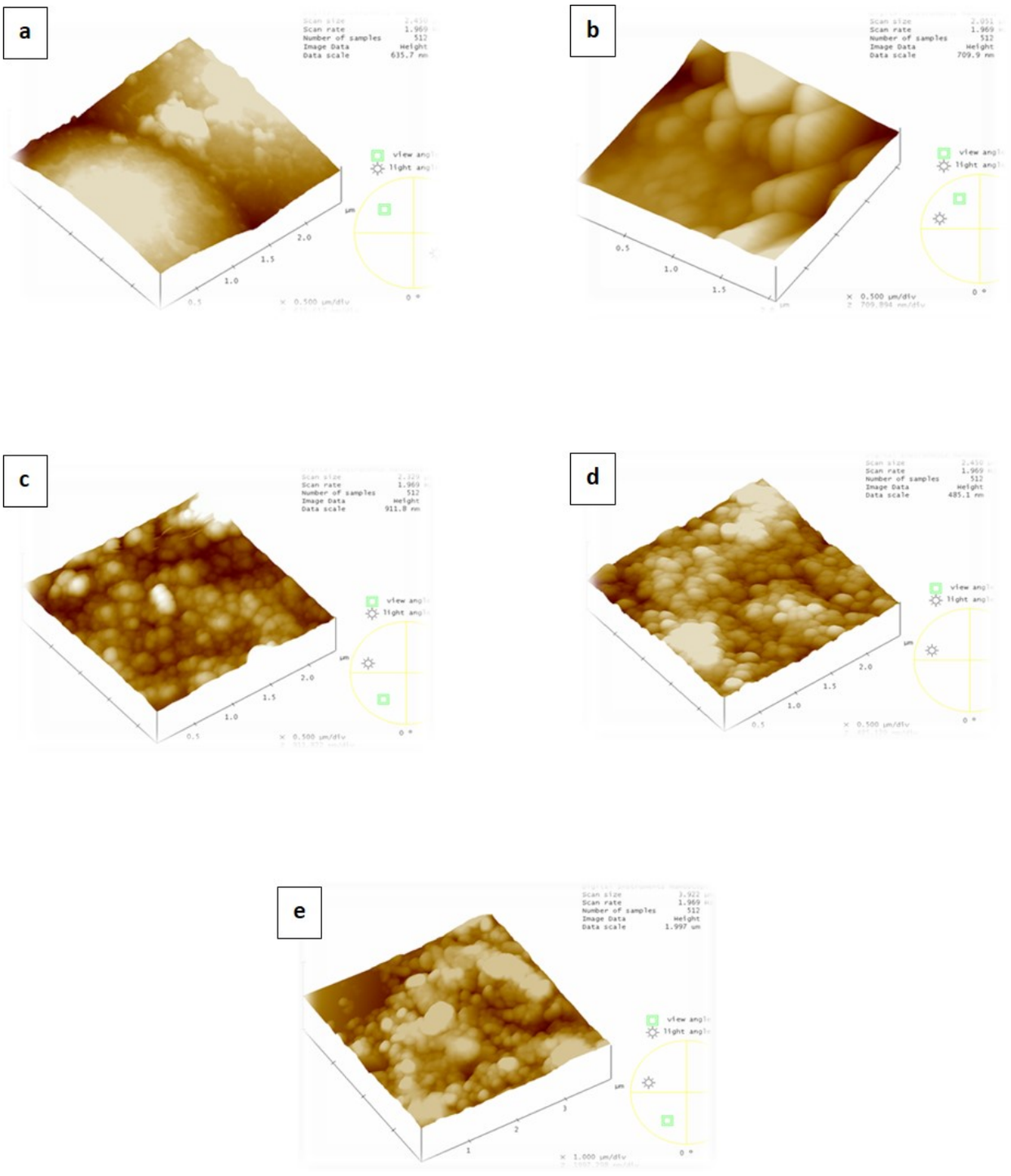

Figure 18. AFM images of Ni-P-SiC electrodeposited onto AISI 1018 steel under galvanostatic conditions (j = 0.021 A/cm^2, t = 20 min) from solution S + 0.084 mM DTAB + 0.02 g mL^{-1} SiC and heat treated at different temperatures: (a) without thermal annealing, (b) 300 °C, (c) 400 °C, (d) 500 °C, and (e) 600 °C.

3.3.3. Tribological properties

3.3.3.1. Microhardness of Ni-P-SiC coatings

Figure 19 shows the surface microhardness of the Ni-P-SiC composites as a function of the annealing temperature. When the annealing temperature was less than 400 °C, a slight increase in the hardness values is observed; however, when the heat treatment was in the range of 400 °C to 500 °C, the hardness value change significantly (from 1057.2 HV to 1453.4 HV). This increase in hardness was associated with a structural change due to the formation of hard intermetallic Ni_3P particles within the Ni-P-SiC coating. The obtained hardness value of the Ni-P-SiC composites at 500 °C (1453.4 HV) is greater than that of a hard Cr coating, which a microhardness value of 1020 HV [24]. Finally, at annealing temperatures above 500 °C, the hardness of the Ni-P-SiC coating decreased sharply. At higher temperatures, the coating began to soften because the Ni_3P particles conglomerated, reducing the number of hardening sites. This process also removes P and SiC from the alloy, producing a separate phase of soft Ni within the matrix and further reducing the bulk hardness.

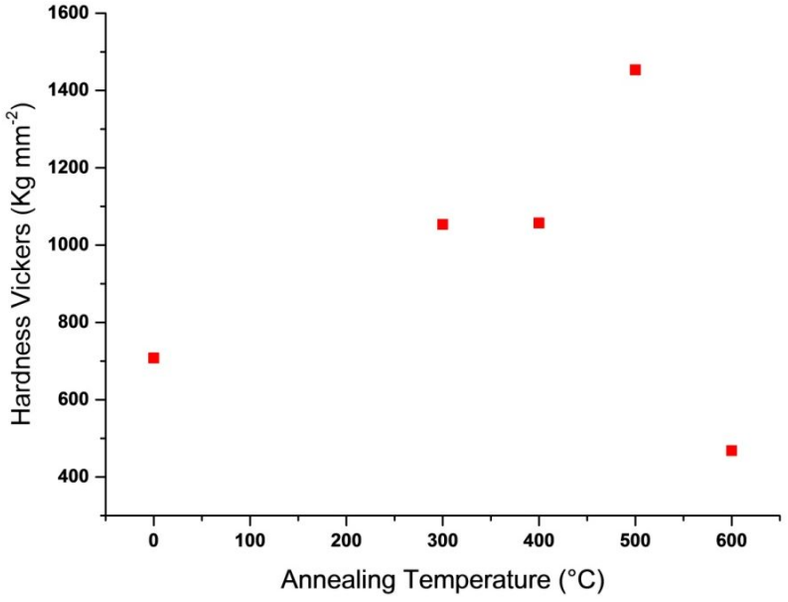

Figure 19. Hardness of the electrodeposited Ni-P-SiC coatings after a 60-min heat treatment.

3.3.3.2. Wear resistance

Figure 20 shows the wear volume of the electrodeposited Ni-P-SiC coatings as a function of the annealing temperature. Once the coating began to harden to approximately 400 °C, the decrease in the wear volume was small. When the coating was heat treated at 500 °C, the wear volume decreased sharply (i.e., the wear resistance increased). The coating that was heat treated at 600 °C contained cracks in its surface that could negatively affect its abrasion resistance.

http://dx.doi.org/10.5772/61858

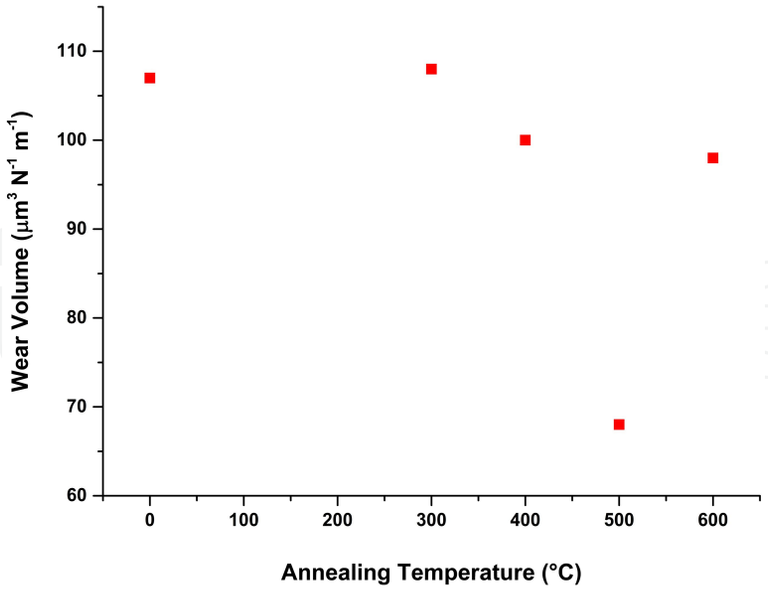

Figure 20. The wear volume of the Ni-P-SiC coatings after a 60-min heat treatment at different temperatures.

3.3.3.3. Friction coefficients

Figure 21 shows the characteristic profile of the coefficient of friction of the Ni-P-SiC coatings without and with heat treatment at different temperatures. When the Ni-P-SiC coatings were treated at temperatures above 200 °C, the coefficient of friction rapidly reached equilibrium. After 1000 cycles, coatings treated at 500 °C had the lowest friction coefficient.

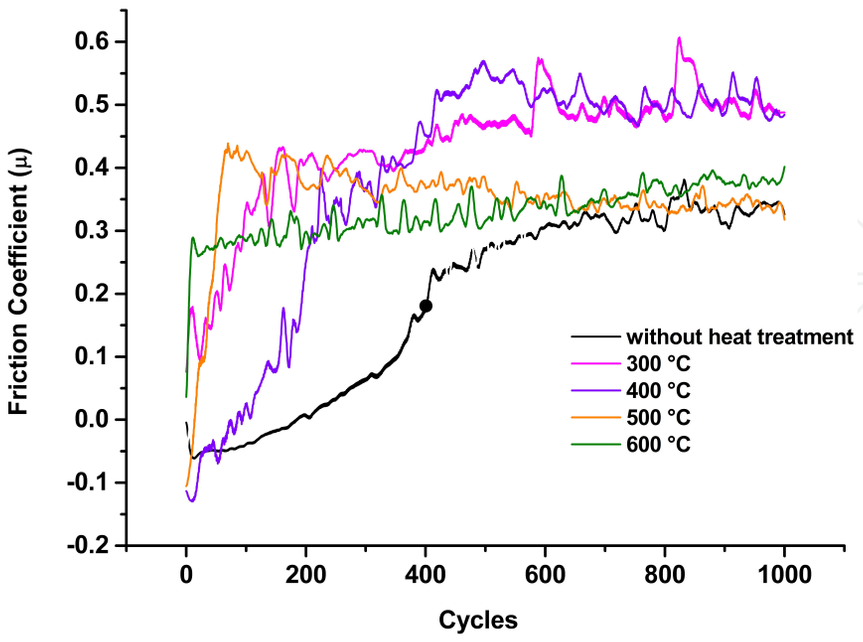

Figure 21. Frictional coefficient for the Ni-P-SiC coatings after a 60-min heat treatment at different temperatures.

4. Conclusions

This work presents the results obtained from a study of the effects of both: SiC dispersion in the metallic matrix and thermal treatment on the tribological characteristics (hardness, wear resistance, and coefficient of friction) of electrodeposited Ni-P-SiC coatings.

Our results show that the dispersion of SiC particles in the metallic matrix improves coating tribological properties such as hardness and wear resistance while diminishing the friction coefficient.

The best results were obtained when a current density of 0.042 A/cm^2 was used in an electrolytic bath containing 0.02 g mL^{-1} of SiC. Such conditions produce a metallic matrix with a concentration of 0.52 at.% SiC particles that in turn increase the Ni-P hardness from 430 HV (for the case when SiC particles are absent) to 600 HV. Despite the observed enhancement in hardness, such values are still below those exhibited by hard Cr coatings (1020 HV).

The XRD results indicated that the Ni-P-SiC composites were amorphous in nature. Thermal treatment between 400 °C and 500 °C changed the microstructure of the Ni-P-SiC matrix from amorphous to crystalline. Thermally treating the Ni-P-SiC coatings at temperatures ≥500 °C transformed the amorphous alloy into a continuous Ni_3P layer containing isolated Ni crystals.

An increased hardness and a decreased wear coefficient were observed after heat treatment for 60 min at 500 °C because of the formation of a Ni_3P phase.

We also observed that the wear volume was inversely proportional to the microhardness of the deposits. As a result, the Ni-P-SiC coatings that were thermally treated at 500 °C possessed the greatest wear resistance; this resistance was superior even to that of hard Cr coatings.

Author details

Alma Martínez-Hernández[1], Federico Manríquez-Guerrero[1], Julieta Torres[1], Raúl Ortega[1], José de Jesús Pérez-Bueno[1], Yunny Meas[1], Gabriel Trejo[1*] and Alia Méndez-Albores[2]

*Address all correspondence to: gtrejo@cideteq.mx

1 Laboratory of Composite Materials and Functional Coatings, Center of Research and Technological Development in Electrochemistry (CIDETEQ), Querétaro, México

2 Center of Chemistry-ICUAP Benemérita Universidad Autónoma de Puebla, Puebla, México

References

[1] Navisek B, Panjan P, Milosev I. PVD coatings as an environmentally clean alternative to electroplating and electroless processes. Surf. Coat. Technol. 1999;116–119:476–487. DOI: 10.1016/S0257-8972(99)000145-0

[2] Heydrzadeh Sohi M, Kashi AA. Comparative tribological study of hard and crack-free electrodeposited chromium coatings. J. Mater. Process. Technol. 2003;138:219–222. DOI: 10.1016/S0924-0136(03)00075-X

[3] Eskin S, Berkh O, Rogalsky G, Zahavi J. Co-W alloys for replacement of conventional hard chromium.. Plat. Surf. Finish. 1998;85:79–83.

[4] Donten M, Casiulis H, Stojek Z. Electrodeposition and properties of Ni-W, Fe-W and Fe-Ni-W amorphous alloys. A comparative study.. Electrochim. Acta. 2000;45:3389–3396. DOI: 10.1016/S0013-4686(00)00437-0

[5] Capel H, Shipway PH, Harris SJ. Sliding wear behaviour of electrodeposited cobalt-tungsten and cobalt-tungsten-iron alloys.. Wear. 2003;255:917–923. DOI: 10.1016/S0043-1648(03)00241-2

[6] Kieback B, Neubrand A, Riedel H. Processing techniques for functionally graded materials. Mater. Sci. Eng. A. 2003;362:81–106. DOI: 10.1016/S0921-5093(03)00578-1

[7] Wang L, Gao Y, Xu T, Xue Q. Graded composition and structure in nanocrystalline Ni–Co alloys for decreasing internal stress and improving tribological properties.. J. Phys. D. Appl. Phys. 2005;38:1318–1324. DOI: 10.1088/0022-3727/38/8/033

[8] Wang L, Gao Y, Xu T, Xue Q. Corrosion resistance and lubricated sliding wear behaviour of novel Ni–P graded alloys as an alternative to hard Cr deposits. Appl. Surf. Sci. 2006;252:7361–7372. DOI: 10.1016/j.apsusc.2005.08.040

[9] D. Nava D, Dávalos CE, Martínez-Hernández A, Manríquez F, Meas Y, Ortega-Borges R., Pérez-Bueno JJ, Trejo G. Effects of heat treatment on the tribological and corrosion properties of electrodeposited Ni-P alloys. Int. J. Electrochem. Sci. 2013;8:2670–2681.

[10] Balaraju JN, Seshadri SK. Synthesis and corrosion behavior of electroless Ni-P-Si_3N_4 composite coatings. J. Materials. Sci. Lett. 1998;17:1297–1299.

[11] Lee Hong-Kee, Lee Ho-Young, Jeon Jun-Mi. Electrolytic deposition behaviors of Ni-SiC composite coatings containing submicron-sized SiC particles. Met. Mater. Int. 2008;14:599–605. DOI: 10.3365/met.mat.2008.10.599

[12] Chou Min-Chieh, Ger Ming-Der, Ke Shih-Tsung, Huang Ya-Ru, Wu Shinn-Tyan. The Ni–P–SiC composite produced by electro-codeposition. Mater. Chem. Phys. 2005;92:146–151. DOI: 10.1016/j.matchemphys.2005.01.021

[13] Guo Ch, Zuo Y, Zao X, Zhao J, Xiong J. The effects of electrodeposition current density on properties of Ni-CNTs composites coatings. Surf. Coat. Technol. 2008;202:3246–3250. DOI: 101016/j.surfcoat.2007.11.032

[14] Pompei E, Magagnin L, Lecis N, Cavallotti PL, Electrodeposition of Nickel-BN composite coatings. Electrochim. Acta. 2009; 54:2571–2574. DOI:10.1016/j.electacta. 2008.06.034

[15] Malfatti CF, Ferreira JZ, Oliveira CT, Rieder ES, Bonino JP. Electrochemical behavior of Ni-P-SiC composite coatings: effect of heat treatment and SiC particle incorporation.. Mater. Corros. 2012;63:36–43. DOI: 10.1002/maco.200905611

[16] Zhang S, Han K, Cheng L. The effect of SiC particles added in electroless Ni–P plating solution on the properties of composite coatings.. Surf. Coat. Technol. 2008;202:2807–2812. DOI: 10.1016/j.surfcoat.2007.10.015

[17] Farzaneh A, Mohammadi M, Ehteshamzadeh M, Mohammadi F. Electrochemical and structural properties of electroless Ni-P-SiC nanocomposite coatings.. Appl. Surf. Sci. 2013;276:679–704. DOI: 10.1016/j.apsusc.2013.03.156.

[18] Hansal WEG, Sandaluche G, Mann R, Leisner P. Pulse-electrodeposited NiP–SiC composite coatings. Electrochim. Acta. 2013;114:851–858. DOI: 10.1016/j.electacta. 2013.08.182

[19] Chen H, Ravishankar S, Farinato R. Rational polymer design for solid–liquid separations in mineral processing applications. Rational polymer design for solid–liquid separations in mineral processing applications. Int. J. Miner. Process. 2003;72:75–86. DOI: 10.1016/S0301-7516(03)00088-7

[20] Nguyen AV, Schulze HJ. Colloidal Science of Flotation. 1st ed. NewYork: Marcel Dekker; 2004. 843 p.

[21] Reyes Y, Suarez R, Ruiz C, Torres J, Mendez A, Trejo G. Electrodeposition, characterization and antibacterial activity of zinc/silver particle composite coatings. Appl. Surf. Sci. 2015; 342: 34–41. DOI: i.org/10.1016/j.apsusc.2015.03.037

[22] Celia C, Trapasso E, Cosco D, Paolino D, Fresta M. Turbiscan Lab® expert analysis of the stability of ethosomes® and ultradeformable liposomes containing a bilayer fluidizing agent. Colloids Surf. B. 2009;72:155–160. DOI: 10.1016/j.colsurfb.2009.03.007

[23] Bordes C, Snabre P, Frances C, Biscans B. Optical investigation of shear- and time-dependent microstructural changes to stabilized and depletion-flocculated concentrated latex sphere suspensions. Power Technol. 2003;130:331–337. DOI: 10.1016/S0032-5910(02)00212-7

[24] Apachitei I Tichelaar FD, Duszczyk J, Katgerman L. The effect of heat treatment on the structure and abrasive wear resistance of autocatalytic NiP and NiP–SiC coatings. Surf. Coat. Technol.. 2002;149:263–278. DOI: 10.1016/S0257-8972(01)014

[25] Zeller RL, Salvati L. Effects of phosphorus on corrosion resistance of electroless nickel in 50% sodium hydroxide. Corrosion. 1994;50:457–467.

[26] Garcia-Alonso MC, Escudero ML, Lopez V, Macias A. The corrosion behaviour of laser treated Ni/P alloy coatings on mild steel. Corros. Sci. 1996;38:515–530. DOI: 10.1016/0010-938X(96)00151-5

[27] Huang YS, Cui FZ. Effect of complexing agent on the morphology and microstructure of electroless deposited Ni–P alloy. Surf. Coat. Technol. 2007;201:5416–5418. DOI: 10.1016/j.surfcoat.2006.07.189

[28] Alirezaei S, Monirvaghefi SM, Salehi M, Saatchi A. Wear behavior of Ni–P and Ni–P–Al_2O_3 electroless coatings. Wear. 2007;262:978–985. DOI: 10.1016/j.wear.2006.10.013

[29] Malfatti CF, Zoppas Ferreira J, Santos CB, Souza BV, Fallavena EP, Vaillant S, Bonino JP. NiP/SiC composite coatings: the effects of particles on the electrochemical behavior. Corros. Sci. 2005;47:567–580. DOI: 10.1016/j.corsci.2004.07.011

[30] Bonino JP, Bruet-Hotellaz S, Bories C, Pouderoux P, Rousset A. Thermal stability of electrodeposited Ni–P alloys. J. Appl. Electrochem. 1997;27:1193–1197. DOI: 10.1023/A:1018423701791

[31] Tachev D, Georgieva J, Armyanov J, C. Magnetothermal study of nanocrystalline particle formation in amorphous electroless Ni-P and No-Me-P alloys. Electrochim. Acta. 2001;47:359–369. DOI: 10.1016/S0013-4686(01)00587-4

[32] Hu Chi-Chang, Bai A. Influences of the phosphorus content on physicochemical properties of nickel–phosphorus deposits. Mater. Chem. Phys. 2002;77:215–225. DOI: 10.1016/S0254-0584(01)00592-2

[33] Bai A, Hu Chi-Chang. Effects of annealing temperatures on the physicochemical properties of nickel–phosphorus deposits. Mater. Chem. Phys. 2003;79:49–57. DOI: 10.1016/S0254-0584(02)00455-8

[34] Keong KG, Sha W, Malinov S. Hardness evolution of electroless nickel–phosphorus deposits with thermal processing. Surf. Coat. Technol.. 2003;168:263–274. DOI: 10.1016/S0257-8972(03)00209-3

[35] Bozzini B, Martini C, Cavallotti PL, Lanzoni E. Relationships among crystallographic structure, mechanical properties and tribological behaviour of electroless Ni–P(9%)/B4C films. Wear. 1999;225–229:806–813. DOI: 10.1016/S0043-1648(98)00389-5

[36] Magdy AM. Black nickel electrodeposition from a modified Watts bath.. J. Appl. Electrochem. 2006;36:295–301. DOI: 10.1007/s10800-005-9077-8

[37] Lewis DB, Marshall GW. Investigation into the structure of electrodeposited nickel-phosphorus alloy deposits. Surf. Coat. Technol. 1996;78:150–156. DOI: 10.1016/0257-8972(94)02402-2

[38] Rabizadeh T, Reza Allahkaram S, Zarebidaki A. An investigation on effects of heat treatment on corrosion properties of Ni–P electroless nano-coatings. Mater. Des. 2010;31:3174–3179. DOI: 10.1016/j.matdes.2010.02.027

[39] Lu K, Sui ML, Lück R. Supersaturation of phosphorus in nanophase nickel crystallized from an amorphous Ni-P alloy. Nanostr. Mater. 1994;4:465–473. DOI: 10.1016/0965-9773(94)90118-X

[40] Serebryakov A, Stelmukh V, Voropaeva L, Novokhatskaya N, Levin Yu. Nanocrystallization of Co/Si/B/Zr amorphous alloy. Nanostr. Mater. 1994;4:645–650. DOI: 10.1016/0965-9773(94)90016-7

[41] Lu K. The thermal instability of nanocrystalline Ni/P materials with different grain sizes. Nanostr. Mater. 1993;2:643–652. DOI: 10.1016/0965-9773(93)90039-E.